Key Engineering Materials
ISSN: 1662-9795, Vol. 926, pp 1505-1515
doi:10.4028/p-09md1c

Submitted: 2021-12-08
Revised: 2022-02-01
Accepted: 2022-02-10
Online: 2022-07-22

Influence of the Surrounding Sheet Geometry on a Clinched Joint

Sven Martin[1,a*], Kristijan Kurtusic[1,b] and Thomas Tröster[1,c]

[1]Paderborn University, Faculty of Mechanical Engineering, Chair of Automotive Lightweight Design, Warburger Str. 100, 33098 Paderborn, Germany

[a]sven.martin@uni-paderborn.de, [b]kurtusic@mail.uni-paderborn.de, [c]thomas.troester@uni-paderborn.de

Keywords: clinched joint, sheet-joint interaction, design method, mechanical joining

Abstract. Point-shaped joints of complex assemblies and components are loaded mainly by shear, whereas the actual load in a joint depends on the surrounding sheet geometry and the number and layout of the joints. Within the scope of this paper, the interaction between a joint and its surrounding geometry is investigated on overlapped single clinched specimens. The geometry in the proximity of the joint is changed by thickening and inserting corrugations and rectangular cavities. The investigations clearly show that the change in geometry, causes different stress states in the joint.

Introduction

Towards the end of the design process, the finalization of a clinched component is done in two steps that can be iterated. After determining the shape and thickness of the sheet metal parts, the number and arrangement of the joints is specified. [1] This practical approach considers the interactions between the joints and the sheet metal parts only indirectly and unilaterally. A more holistic design method would modify the joint layout and the geometry of the component simultaneously. Understanding the interaction between the joint and its proximity is a fundamental requirement to establish such a method and is consequently investigated here.

From the determination of mechanical characteristics of joints, it is known that the geometry of the specimen has an influence on the measured force-displacement curve. Therefore, the specimens for testing point-shaped joining elements are made as stiff as possible. The error made during the measurement is higher in the head tension than in the shear tension test. [2] In [1], three common methods to optimize the distribution of joints using finite element models are shown and it is recommended to use the joint topology optimization. In [3] it is shown that the distribution of joints can also be determined with the use of supervised machine learning. An algorithm has been trained with a dataset of joining scenarios derived from CAD data of thirteen different vehicles. The joint topology optimization and the supervised learning approach have the drawback that the joint distribution is changed, but the sheet metal components remain unchanged. With the multi-material multi-joint topology optimization of [4], the sheets and the joints are optimized simultaneously. This approach is further developed for considering tooling accessibility [5]. Another disadvantage of the topology optimization and the machine learning approach is the lack of feedback to the user during the optimization. Since the user cannot see a physical criterium for the absence or presence of a joint is very difficult to derive a cause-effect relationship between the surrounding sheet geometry and the loading in the joint.

One method that has the potential to show such relationships is the load path method. In previous work [6], it is indicated that the load path transmission could be used for the optimization of structures and joints. The aim is to use the load path analysis to improve the joint design of a clinched component by optimizing either the sheet geometry, the clinched joints themselves or both simultaneously. In [7], Steinfelder and Brosius introduce a load path analysis approach which is independent of the alignment of the specimen.

Instead of using the load path analysis, the load in the joints and in the sheets can be determined with physical quantities provided directly by the postprocessor of a finite element software. In this study, the von Mises stress and nodal forces are used to investigate how the sheet geometry in the

proximity of the clinched joint affects the load in the joint. The different load distribution in the sheets is represented by the internal energy density.

Method

The method, the test setup and the shape of the specimen described in this section are based on the aim of identifying the interaction between the joint load and sheet geometries. Since point-shaped joints in an assembly are mainly loaded by shear [8], a test-setup which ensures that the joint is mainly loaded by shear is chosen. Since only the force acting in x-direction in the specimen and the deformation and displacement and the surface can be measured in an experiment, an evaluation of a simulated test is preferred. In simulation results, the loads in the joint and in the sheet can be displayed and thus areas with higher and lower loads can be identified. With the presented method, it is possible to see how a change in geometry affects the local loads in the sheets and in the clinched joint.

Specimen. The geometry of the specimen can be seen in its initial configuration in Fig. 1. It is made from two sheets of cold-rolled dual-phase steel HCT590x with a thickness of 1.5 mm. During the test, the specimen is clamped on both non-overlapped sides in the device as shown in Fig. 2. In the overlapped area, marked in yellow, the geometry gets modified to achieve a different load in the clinched joint.

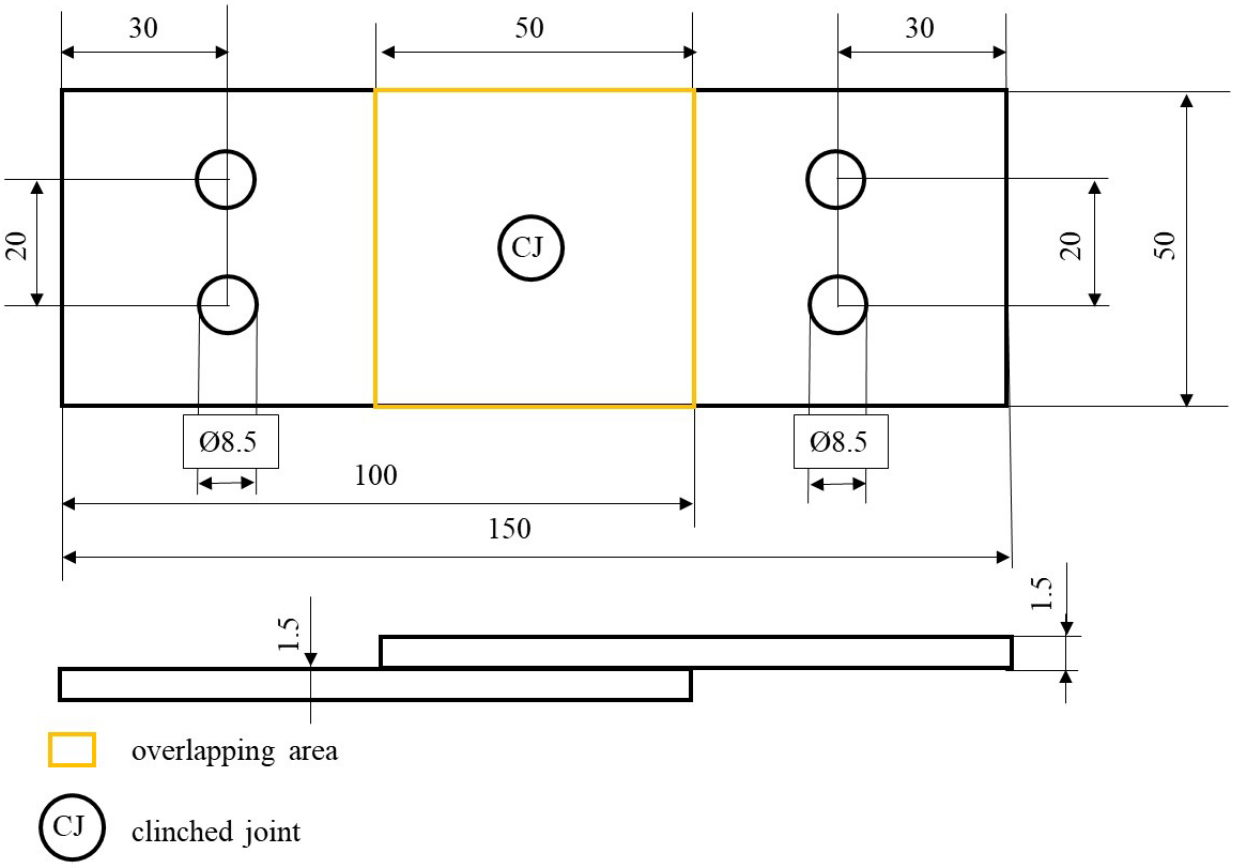

Figure 1: Specimen geometry with yellow marked overlapping area

Experimental Testing. The specimens are tested using the device, which is shown in Fig. 2. It is inspired by a fixture from a standard of the American Society for Testing and Materials (ASTM) which is used for testing notched specimens when characterizing the shear properties of composites [9].

In the following, the coordinate system, which is drawn in Fig. 2, is used. The z-direction is horizontal in the direction of the long edge and the x-direction is vertical in the direction of the short edge of the specimen. The y-direction is perpendicular to the specimen plane. In the overlapping area,

the specimen (5) can move freely in all directions when clamped to the device. The fixation to the specimen holders is done via wedges (3) and blank holders. The specimen holder on the right (2, larger z-value) can move in x-direction relative to the specimen holder on the left (1, lower z-value). This translation is guided by a column frame (6) with two linear ball bearings to ensure that the friction is kept to a minimum. During the experiments, the lower sheet (7) is mounted to a fixture. Then both fixtures are inserted into the universal testing machine and tightened. The displacement of the specimen (5) is applied by moving the specimen holder (1) in the x-direction with a speed of 0.5 mm/min. Due to this arrangement, the specimen is subjected to a minor torsional moment. The deformation of the specimen is measured optically via digital image correlation (DIC) using a GOM Aramis 5M system. For this reason, a stochastic black-white pattern is applied to the specimens, before testing. Dots are stuck on the lower sheet of the specimen to measure a possible rigid body rotation. The resulting displacement in the x-direction is subtracted from the x-displacement of the specimen, ensuring that the movement of the specimen is measured exclusively. The displacement on the specimen surface is detected by an optical measuring system.

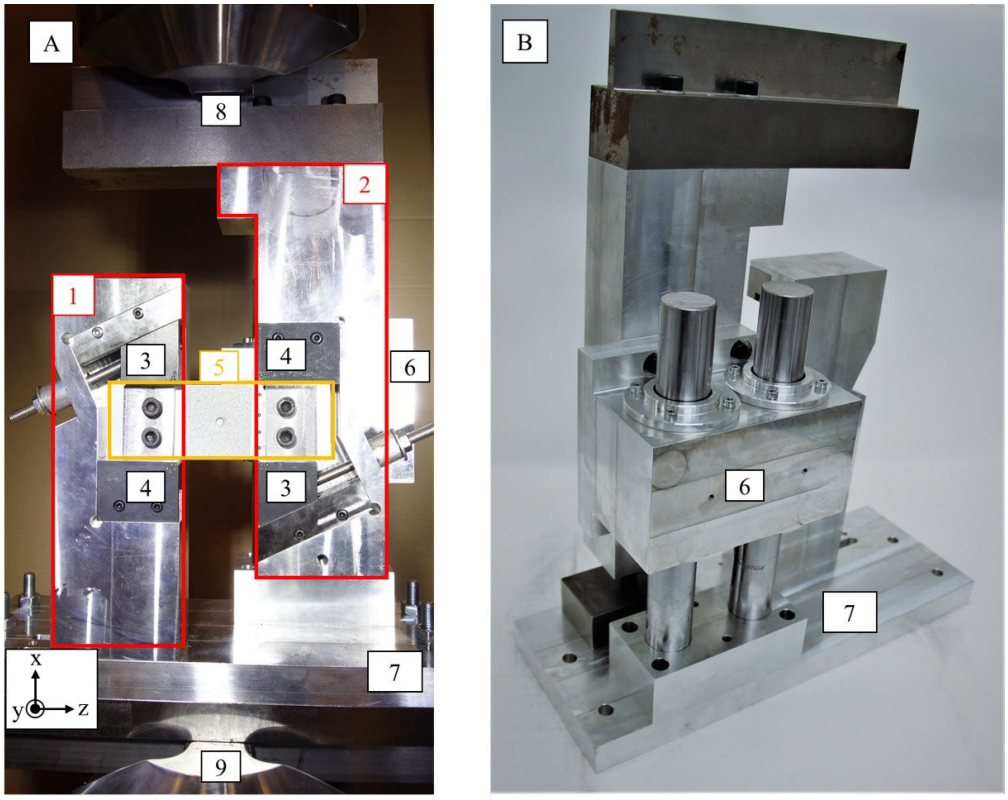

1: left specimen holder
2: right specimen holder
3: wedges
4: contact block
5: specimen
6: column frame
7: bottom plate
8: upper fixture
9: lower fixture

Figure 2: Testing device in frontal view when tightened in a universal testing machine (A) and from behind in isometric view (B)

Finite Element Models. The set-up of the model is shown in Fig. 3. The sheets are represented with hexahedron solid elements and are assigned to a material curve using the Johnson-Cook plasticity model. The curve fit was done comparing force-displacement curves of tensile specimens for the dual-phase steel HCT590X. Damage or failure of the steel is not considered. The clinched joint is modeled with solid elements and contains the stress- and strain-state from the previous forming process. For this purpose, the forming process is calculated 2D rotationally symmetrically in an FE-simulation. The resulting mesh is then rotated 360° and the strain and stress values are mapped. The used material model is the same as for the sheets and the entire workflow is explained in detail

and validated in [10] and [11]. The clinched joint mesh is shown Fig. 6 A. In Fig. 6 B, the pre-stresses are plotted.

The mesh of the initial sheet geometries and the test set-up is depicted in Fig. 3. The translational edge length of the elements is approx. 0.5 mm and 0.2 mm across the sheet plane. All translational displacements of the nodes on the right edge of the lower sheet are constrained (highlighted in yellow). A linear displacement in the x-direction is applied to the nodes of the left edge of the upper sheet (highlighted in green). The meshes of the sheets and the meshes of the joint are connected via tied contact. In the contact modeling between the sheets and the clinched joint, the coefficient of friction is 0.1. The calculation is done in the implicit Solver of LS-DYNA R12.

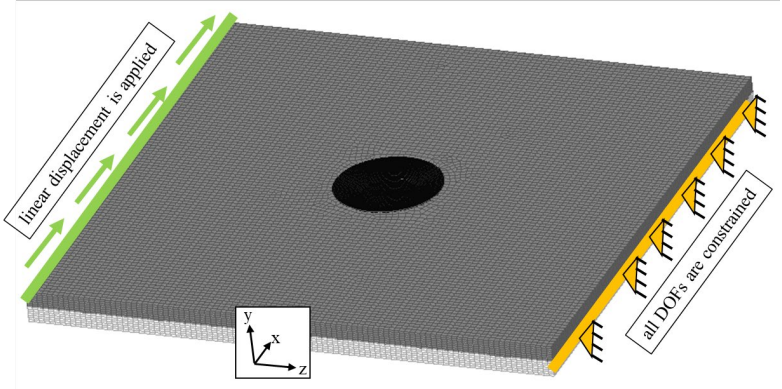

Figure 3: Finite element model for virtual testing

Model Validation. The test with the initial specimen without any geometric changes is executed both experimentally and numerically. Since the ideal clamping as in Fig. 3 is not given in the experiment, the unclamped area was extended in the simulation for this comparison. The force-displacement curves of the experimental test and the simulation are shown in Fig. 4. The measured force in the load cell in the test corresponds to the measurement of the x-force in the constraints in the simulation. As can be seen in Fig. 4, it can be concluded that the simulation represents the force-displacement curve. The initial stiffness and the maximum force are mapped with high accuracy. In the range between 0.07 mm and 0.25 mm, the simulated curve does not match with the experiments. It is highly assumed that external deformations in the test set were also measured, since when simulating an ordinary shear test the experimental and numerical curves fit very well.

The simulation is further validated by comparing the normal displacement of the specimen on the surface. In Fig. 5 A, the numerical and in Fig. 5 B, the measured normal displacement is depicted. In the simulation results (Fig. 5 A), the area measured in the test is highlighted with a black frame. Due to the high agreement of the transversal displacement and the force curve, the model is valid.

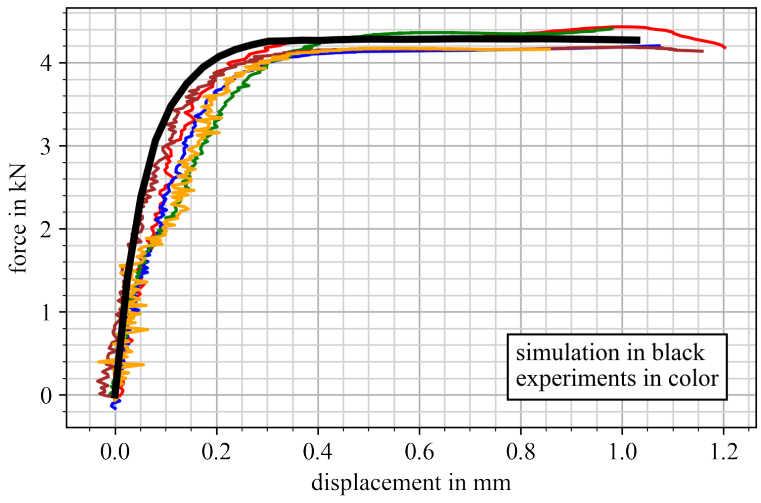

Figure 4: Force-displacement curves of the initial specimen

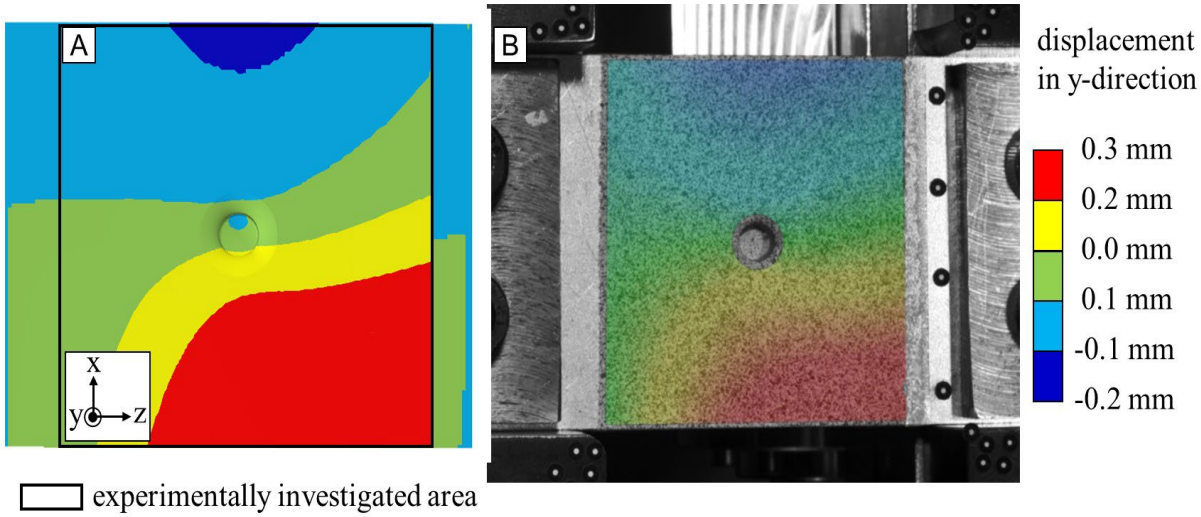

Figure 5: Simulated (A) and measured (B) normal displacement with an applied displacement of 0.2 mm in x-direction

Evaluation of the Load. The internal deformation energy density can be used to identify the load-bearing areas in an elastically deformed component and is therefore used to describe the load in the sheets. Since the joint is plastically deformed due to the joining process, the maximum von Mises stresses are used in the joint to describe the load. The force acting in the clinched joint is the sum of the residual forces of the nodes on the circular surface of the upper part of the clinched joint, as shown in Fig. 6 C.

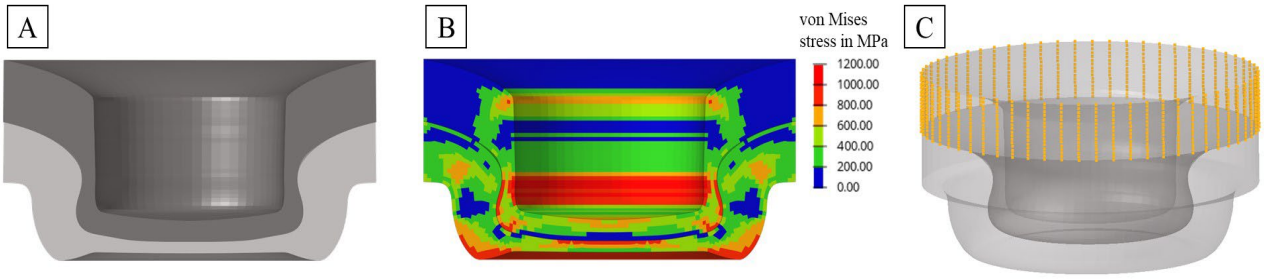

Figure 6:Section in the middle of the clinched joint (A), initial stress in the clinched joint (B) in the section and highlighted nodes to calculate the resulting force in the clinched joint (C)

Investigated Geometries. To investigate how the geometry of the specimen influences the load in the joint, the geometry is changed in three different ways. The variations are shown in Fig. 7. In the first variation, the upper sheet is thickened as seen in A. Then a rectangular cavity is inserted in the upper sheet and the position is varied (B, C). In the last specimen type, there are corrugations on the upper and lower sheet as shown in Fig. 7 D and Fig. 7 E. The corrugations from Fig. 7 E are orientated at 90° to the corrugations of Fig. 7 D. The dimensions of the corrugations are given in Fig. 7 F.

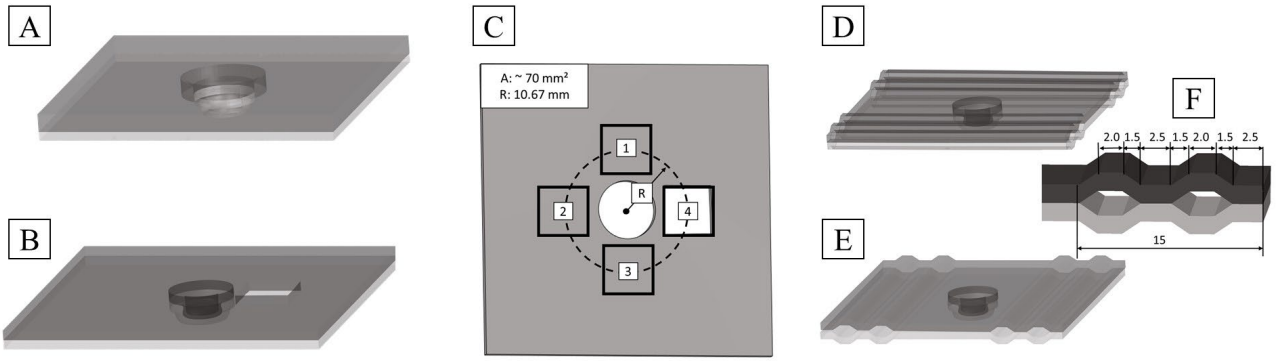

Figure 7: Variations of the simulated specimen: A: Thickened upper sheet, B: Upper sheet with rectangular cavity, C: Positions of the cavities, D: Corrugations translational to the applied displacement, E: Corrugations parallel to the applied displacement, D: Dimensions of the corrugations

Results

The results of the virtual testing are presented in the same order as the specimens' geometries in Fig. 7.

Initial Specimen. Based on the clinched joint force components, the general sequence of the virtual test is explained. At the beginning, there is a force in the y-direction (in the direction of thickness) due to the joint's preload in the normal direction, which degrades to zero during testing. By moving the upper sheet in the x-direction, the inner contact surfaces in the clinched joint get in contact with each other and a force is induced in the x-direction. This force component is measured in the experimental test. At the same time, the eccentric application of the displacement causes a torsional moment, which generates a force in the z-direction. The force generated by the moment is approximal ten times smaller than the force in the x-direction. The forces at an applied displacement of 0.2 mm can be found in Table 1.

In the following, the loads in the sheets and in the joints are analyzed one after the other. The contour plot of the energy density in the sheets of the initial specimen is depicted in Fig. 8. To ensure that the areas of high energy density are not hidden by other elements, all elements with a density below the value of 0.0125 J/mm³ are hidden.

Looking at the upper sheet (Fig. 8 A and C), four observations can be made. In general, the areas with higher energy density are near the surfaces (I). Areas of high energy density are located near the clamping (II). The larger areas of high energy density in the immediate proximity of the joint are located on the top surface on the right and on the bottom surface on the left (z-direction) (III). In the corners on the right (z-direction) of the upper sheet, the energy density is below the threshold over the entire thickness. In combination with the displacement plot in the y-direction of Fig. 5, it is concluded that those areas do not bear any load and perform a rigid body motion.

The energy density distribution of the lower sheet is shown in Fig. 8 B and D. There are three main observations. A large proportion of the lower sheet is only barely loaded (I). In the near-surface regions of the top surface, which is the contact surface, much plastic deformation takes place, which can be seen by the high energy density (II). In the bottom near-surface region, there is only a small area that absorbs energy (III).

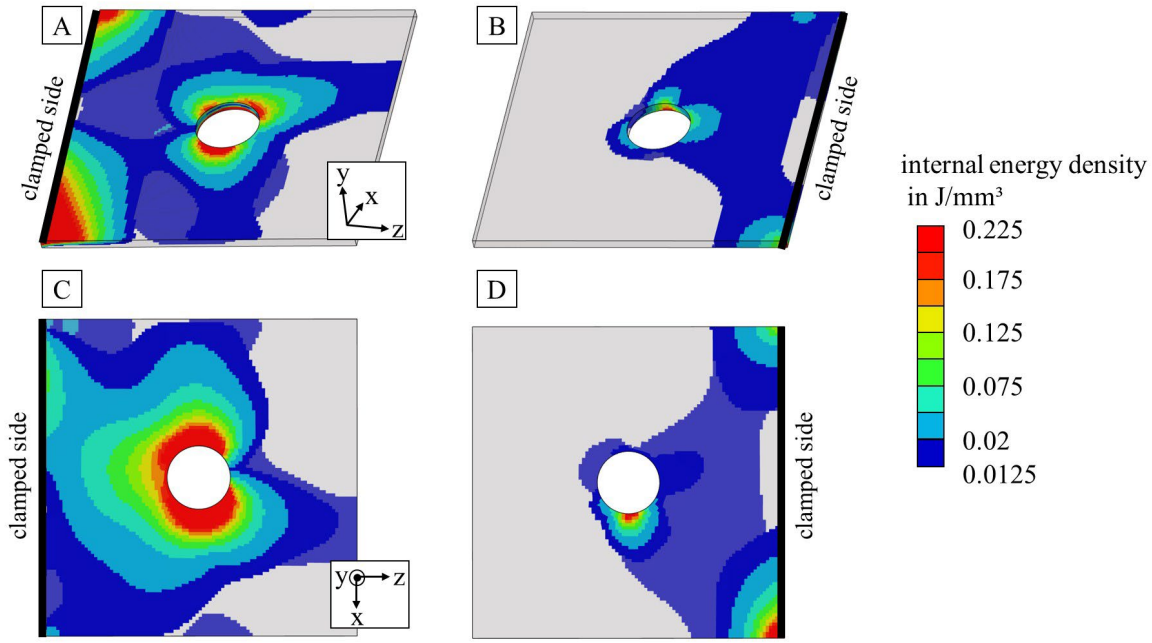

Figure 8: Contour plot of the internal energy density of the initial specimen with an applied displacement of 0.2 mm in x-direction. The filter is set to 0.0125 J. A: Upper sheet, B: Lower sheet, C: Bottom view of the upper sheet, D: Bottom view of the lower sheet

Thickened Upper Sheet. The thickening of the upper sheet significantly changes the energy density distribution in the sheets, as can be seen in Fig. 9. The size of the areas in which the internal energy density is below 0.0125 J/mm³ increases strongly. In both sheets, the area between the clinched joint and the free edge is barely loaded.

In the upper sheet, the areas with an energy density above the threshold are smaller than in the initial model with the thinner upper sheet, as can be seen in Fig. 9 A and Fig 9 C. Furthermore, the distribution of internal energy above 0.0125 J/mm³ in the top surface is nearly mirror symmetric to the x-axis. Looking at the energy density of the upper sheet from the bottom, as in Fig. 9 C, it is also noticeable that the deformation near the bottom is significantly lower. Not shown is the y-displacement, as in Fig. 5, which is significantly smaller in the thickened upper sheet than in the upper sheet with initial thickness.

In the lower sheet, Fig. 9 B and D, there are three significant changes in the energy density plot. In the lower sheet of the initial model, an area above (x-direction) the clinched joint can be seen in which the energy is high over the entire thickness. The closer to the bottom surface, the higher is the internal energy. In the model with the thickened upper sheet, the area with the energy densities above 0.2 J/mm³ on the top surface is significantly smaller (I). The second area with the high energy densities to the right of the clinched joint (y and z-direction) is completely shifted from the top to the bottom surface (II). Overall, the sum of the areas with an energy density above 0.0125 J/mm³ increases significantly. This rearrangement results in a different load behavior of the clinched joint, which is investigated in the following.

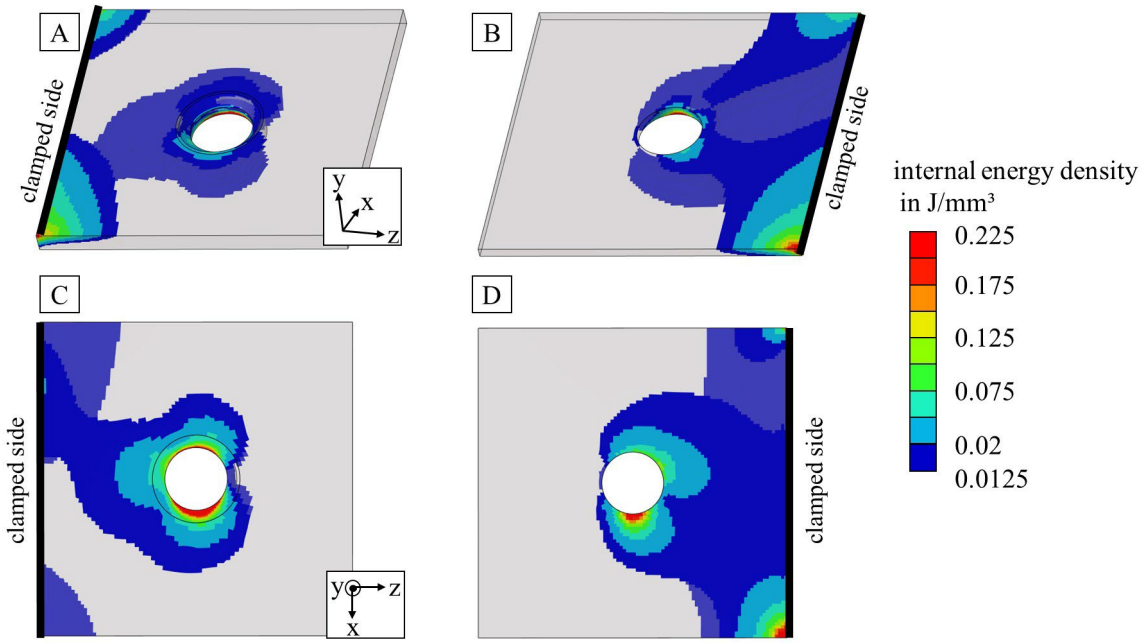

Figure 9: Contour plot of the internal energy density of the specimen with the thickened upper sheet with an applied displacement of 0.2 mm in x-direction. The filter is set to 0.0125 J. A: Upper sheet, B: Lower sheet, C: Bottom view of the upper sheet, D: Bottom view of the lower sheet

Due to the thickening of the upper sheet, the force in the clinched joint increases, as seen in Table 1. In the rear-bottom of the joint, the von Mises stress increases heavily. In Fig. 10, the von Mises stress in the bottom of the upper part of the joint for the test with the initial specimen (A) and the specimen with the thickened upper sheet (B) are shown. For clarity, the elements with a value of less than 650 MPa are masked out. It can be clearly seen that the load in the interlock, which is a critical failure area, is significantly higher than without the thickening.

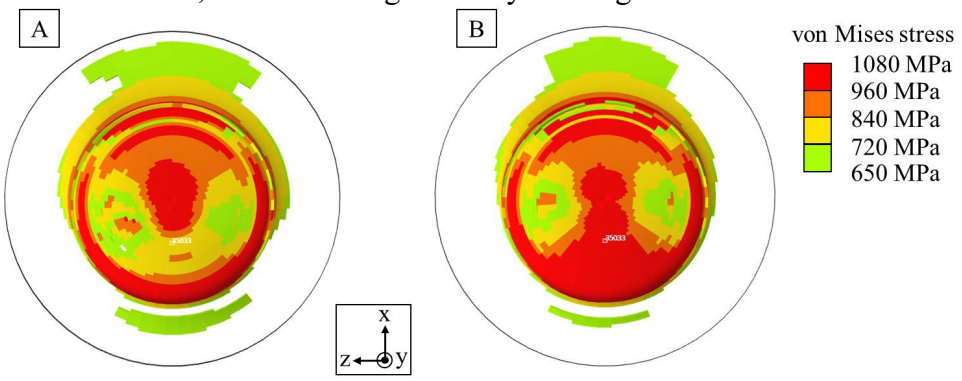

Figure 10: Von Mises stress in the upper part of the clinched joint in bottom view of the initial model (A) and of the model with thickened upper sheet (B) The elements with a stress from equal or lower 650 MPa are masked out.

Rectangular Cavity and Corrugations. By the insertion of corrugations or rectangular cavities, the internal energy density distribution in the sheets changes. The contour plot of the internal energy density for the specimens with corrugations are illustrated in Fig. 11. The energy density plot in the immediate proximity of the clinched joint is very similar. The further radially away from the joint the energy density is observed, the greater is the difference in energy distribution compared to the distribution of the initial specimen in Fig. 8.

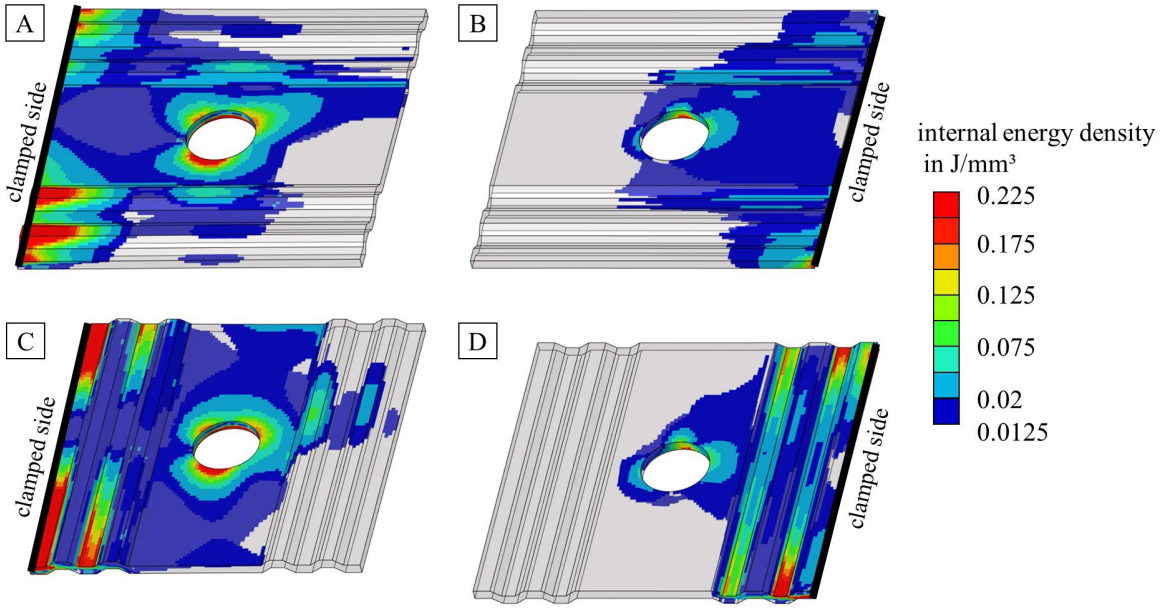

Figure 11: Contour plot of the internal energy density of the specimens with corrugations at a displacement of 0.2 mm in x-direction. The filter is set to 0.0125 J. A: Upper sheet of the specimen with translational corrugations, B: Lower sheet of the specimen with translational corrugations, C: Upper sheet of the specimen with parallel corrugations, D: Lower sheet of the specimen with parallel corrugations

The internal energy density plots with the rectangular cavities are similar to those shown in Fig. 8. No deformation occurs in the cavities, which means that the energy density is zero at those positions. Only a few slight differences in the energy density plots compared to the initial one are identifiable. The clinched joint force, calculated from the sum of the nodes according to Fig. 6 C, changes significantly.

The force components acting on the clinched joint for all described specimens are listed in Table 1. The percentage changes in the force components are illustrated in Fig. 12. In addition, the changes of the load and orientation angle are described in Table 1. The load angle α is the angle between the resulting shear and normal component. A load angle α of 0 indicates that the clinched joint is loaded only by shear.

The orientation angle β is the angle between the z-axis and the resulting shear force. The maximum change in the orientation angle β is a change of approximately minus five degrees. A change in the orientation angle β means that the direction in the sheet plane, from which the shear force is acting on the joint, changes. The change in the direction of the shear force component in the joint results from different displacement conditions on the joint in the sheet plane (x and z-displacement) caused by the different geometry.

Table 1: Force components, load angle α, orientation angle β in the clinched joint of all specimens

	force component (N)			angle (°)	
	x-force	z-force	y-force	load angle α	orientation angle β
initial	3940	345	58	0,8	85.0
thickened	4185	485	-49	-0,7	83.4
parallel	3894	608	88	1,3	81.1
translational	4059	532	29	0,4	82.5
cavity #1	3854	679	28	0,4	80.0
cavity #2	3869	-161	59	0,9	92.4
cavity #3	3872	134	88	1,3	88.0
cavity #4	4017	255	50	0,7	86.4

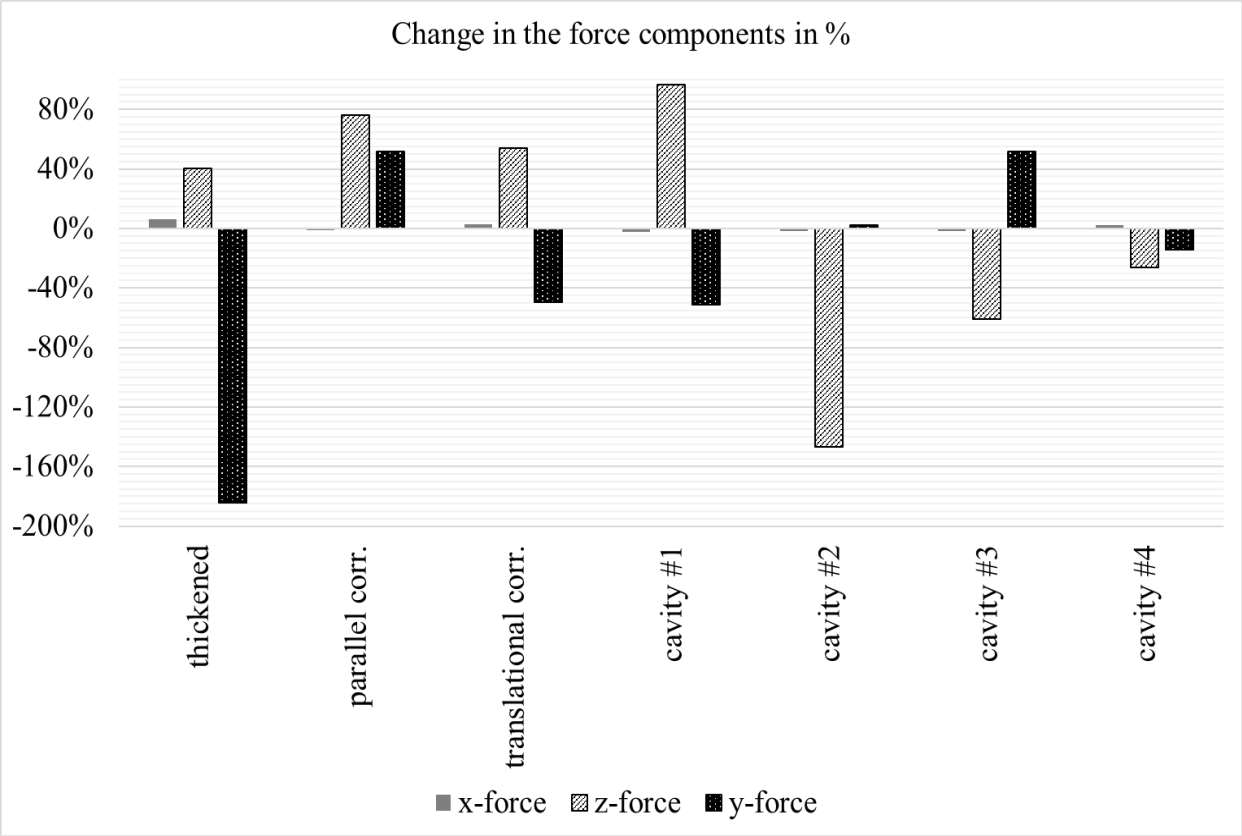

Figure 12: Percentage changes in the force components in relation to the initial model

Discussion. The results show that in a displacement-controlled motion, the geometry in the sheet in the proximity of the joint influences the deformation in the sheet and thus the displacement acting on the joint. This different displacement affects the contact behavior, the tilting of the joint and so the stresses in the joint. Hence, the transmitted force changes its magnitude and its direction.

For example, due to the higher stiffness of the thickened sheet, the displacement of the upper part of the clinched joint in the x-direction is higher. After thickening, the upper part of the clinched joint moves almost exclusively in the x-direction and is hardly tilted at all. At the same time, the bottom part of the clinched joint, moves more in the negative y-direction when the upper sheet is thickened. In particular, the lower part of the clinched joint also moves much more in negative y-direction in the rear contact area. In summary, if both sheets have the same thickness, the upper part of the joint is tilting and if the upper sheet is thickened, the lower part of the joint is tilting. It is plausible that the different movement causes a change in the magnitude of the force in the y-direction.

In addition to the thickened specimen, the specimen with the perpendicular corrugations also has a higher bending stiffness in the upper sheet. Here, both effects, the movement of the lower part of the joint against the y-direction and the decrease of the y-force component is observed.

The influence of the cavities depends on their position. The effect of the cavities in front (#1) and behind (#3) of the clinched joint is contrary to the symmetry of the applied testing. Their effects are vice versa and the change in the y-force component has even the same absolute value. The change in the z-force component is higher for cavity #1. Since the cavity #1 is located in a higher loaded area than cavity #3 and at the same time, the percentage change of the z-force is higher and the absolute change of the y-force is equal (30 N), it can be concluded that the displacements in the z-direction in the specimens in front of the clinched joint are larger than behind the joint. Due to the different directions of the change, it is concluded that the z-displacement acts in front of the joint (at the location of cavity #1) in the positive and behind the joint (at the location of cavity #3) in the negative

z-direction. Since the z-displacements are larger behind the clinched joint, the change in the z-force component is smaller when inserting cavity #3 than when inserting cavity #1.

Additionally, the insertion of cavities #2 and #4 also changes the z-force. To understand this phenomenon, further studies should evaluate the x and z displacements over the entire thickness of the sheets. In addition, the stress states in the neck and interlock area must be evaluated over the radius to be able to clearly visualize the load redistribution in the joint.

Comparing the force values of the simulations in Table 1 with the test results from Fig. 4, it is apparent that the changes in the x-force components are smaller than the scatter in the measured force values. In addition, no z-force component can be measured with the current test setup. For this reason, further investigations must be carried out on another test set-up.

Conclusions

The results show that for displacement-controlled loading on a clinched joint, the surrounding geometry has an influence on the stress distribution in the joint. These changes can be explained by the different displacements occurring on the clinched joint due to the change in geometry. In further research, the load redistribution in the neck and the interlock of the joint must be investigated systematically, as these are the critical failure areas. Additionally, the displacements in x- and z-direction in the sheets should be evaluated to clearly understand the effect of the cavities.

Acknowledgement

The funding by the Deutsche Forschungsgemeinschaft (DFG, German Research Foundation) – TRR 285 – Project-ID 418701707, subproject B01 is gratefully acknowledged. Thanks, are also due to the Paderborn Center for Parallel Computing (PC2) for funding this project with the computing time provided. I would also like to thank Max Böhnke and Christian Bielak from the Laboratory for Material and Joining Technology, Department of Mechanical Engineering, Paderborn University for providing a rotated clinched joint model and a material card.

References

[1] A.-B. Ryberg, L. Nilsson Spot weld reduction methods for automotive structures, Struct. Multidiscipl. Optim. 53 (2016), 923–934.

[2] A. Breda, S. Coppieters, D. Debruyne, Equivalent modelling strategy for a clinched joint using a simple calibration method, Thin-Walled Struct. 113 (2017) 1-12.

[3] D.H.D. Eggink, D.F. Perez-Ramirez and M.W. Groll, Automated joining element design by predicting spot-weld locations using 3D convolutional neural networks, 2020 IEEE International Conference on Engineering, Technology and Innovation (ICE/ITMC).

[4] C. Woischwill, I.Y. Kim, Multimaterial multijoint topology optimization, Int. J. Numer. Methods Eng. 115(13) (2018) 1552-1579.

[5] V. Florea, M. Pamwar, B. Sangha, I.Y. Kim, 3D multi-material and multi-joint topology optimization with tooling accessibility constraints, Struct. Multidisc. Optim. 60 (2019) 2531–2558.

[6] C. Steinfelder, S. Martin, A. Brosius, T. Tröster, Load Path Transmission in Joining Elements, Key Eng. Mater. 883 (2021) 73-80.

[7] C. Steinfelder, A. Brosius, A New Approach for the Evaluation of Component and Joint Loads Based on Load Path Analysis, in: B.A. Behrens, A. Brosius, W. Hintze, S. Ihlenfeldt, J.P. Wulfsberg (Eds) Production at the leading edge of technology. WGP, Dresden, 2020

[8] S. Martin, A.A. Camberg, T. Tröster, Probability Distribution of Joint Point Loadings in Car Body Structures under Global Bending and Torsion. Procedia Manuf. 47 (2020) 419-424.

[9] Standard Test Method for Shear Properties of Composite Materials by the V-Notched Beam Method. ASTM D 5379D 5379M – 98

[10] C.R. Bielak, M. Böhnke, R. Beck, M. Bobbert, G. Meschut, Numerical analysis of the robustness of clinching process considering the pre-forming of the parts, J. Adv. Join. Process 3 (2021) 100038.

[11] C.R. Bielak, M. Böhnke, R. Beck, M. Bobbert, G. Meschut, Further development of a numerical method for analyzing the load capacity of clinched joints in versatile process chains, 2020 24th International Conference on Material Forming.